RSC Advances

PAPER

View Article Online
View Journal | View Issue

Cite this: *RSC Adv.*, 2024, **14**, 20398

Analyzing the impact of the size of fluoro and chloro substituents on induced mesomorphism in hydrogen bonded liquid crystals†

M. K. Sonali,[a] Rajeev K. Sinha,[b] Silpa Elizabeth Peter,[a] N. V. Anil Kumar,[a] Nirmal Mazumder,[c] Sindhoora Kaniyala Melanthota,[c] Mohammed Azeezulla Nazrulla[a] and Poornima Bhagavath *[a]

Synthesis of new supramolecules with specific properties and realistic applications requires a sound knowledge of the structure–property relationships of the synthesized molecules. Non-covalent interaction like hydrogen bonding is conducive in realizing mesomorphism. The induction of the liquid crystalline character is associated with the strength of hydrogen bonds formed between the interacting components, which are affected by the change of polarity and polarizability of both components upon change in their terminal polar substituents. When the polar substituents are similar in their reactivity, how does the size of the polar substituent influence the mesomorphism? New hydrogen bonded liquid crystals are synthesized with fluorine and chlorine as substituents, and the mesomorphic behaviour is studied with the size of the substituent as a critical parameter. The chemical characterization is carried out by FTIR measurements, the phase characterization by polarizing optical microscopy and the thermal characterization by differential scanning calorimetry. The DFT method utilizing wb97x-D theory along with the cc-pVTZ basis set were used for the calculations. The hybrid functional B3LYP-D3 and Gaussian type basis set 6-31G(d,p) were used for studying the orientation of the molecules. It is observed that the *ortho* substituents reduce the co-planarity, *meta* substituents lead to the molecular broadening while *para* substituents exhibited highest mesomorphism by enhancing longitudinal dipole moment. Fluoro substituted compounds are exhibiting higher mesomorphism while the bulky chloro substituents are helping to better stack the molecules possessing longer chain lengths.

Received 14th December 2023
Accepted 22nd May 2024

DOI: 10.1039/d3ra08569d

rsc.li/rsc-advances

1. Introduction

Display materials have been at the forefront of condensed matter research for many years. The anisotropic properties and energy storage capabilities of liquid crystals make them valuable for providing color to digital displays and semiconductor applications without the need for conduction. Liquid crystals exhibit mesomorphism, a phase of matter intermediate between a solid and liquid. Supramolecular liquid crystalline systems can be synthesized by combining hydrogen bond donors and acceptors. This method enables the synthesis of self-assembled systems that stack through non-covalent forces. A network of complementary molecules can create mesophases even with a combination of non-mesogenic donors and acceptors by enhancing the longitudinal dipole moment.[1–7] Hydrogen-bonded liquid crystals (HBLCs) obtained using nOBAs showed increased stability in the tilted phase.[8] The association between a basic pyridine derivative and an acidic moiety creates liquid crystalline phases with various polymorphisms, such as SmC, SmA, SmF, SmG, SmI, nematic, and discotic phases, based on their donor–acceptor interactions through intermolecular hydrogen bonding.[9–11]

Pyridyl derivatives hydrogen-bonded with halo-substituted acids exhibit mesomorphism, forming hetero-synthons. The size and position of substituents significantly affect the thermal stability of benzoic acid complexes. Smaller substituents result in higher mesomorphic stability, melting, and clearing temperatures. The *meta*-substituted benzoic acid exhibit lowest thermal range of mesomorphism, while *para*-substituted ones show higher thermal ranges.[12] Although there are reports on the nature and position of the substituents influencing mesomorphism, the information regarding the impact of substituent size is meagre.[13–20] Our present study explores the effects of both size and position of halo substituents on the mesomorphic behaviour of HBLCs. By optimizing the structure with octyl and octadecyl carbon chain lengths, we analyze the interactions of proton acceptors P8 and P18 with fluoro and chloro-substituted

[a]*Department of Chemistry, Manipal Institute of Technology, Manipal Academy of Higher Education, Manipal, 576 104, Karnataka, India. E-mail: poornima.nayak@manipal.edu*

[b]*Department of Physics, Birla Institute of Technology Mesra, Ranchi-835215, Jharkhand, India*

[c]*Department of Biophysics, Manipal School of Life Sciences, Manipal Academy of Higher Education, Manipal, Karnataka, 576104, India*

† Electronic supplementary information (ESI) available. See DOI: https://doi.org/10.1039/d3ra08569d

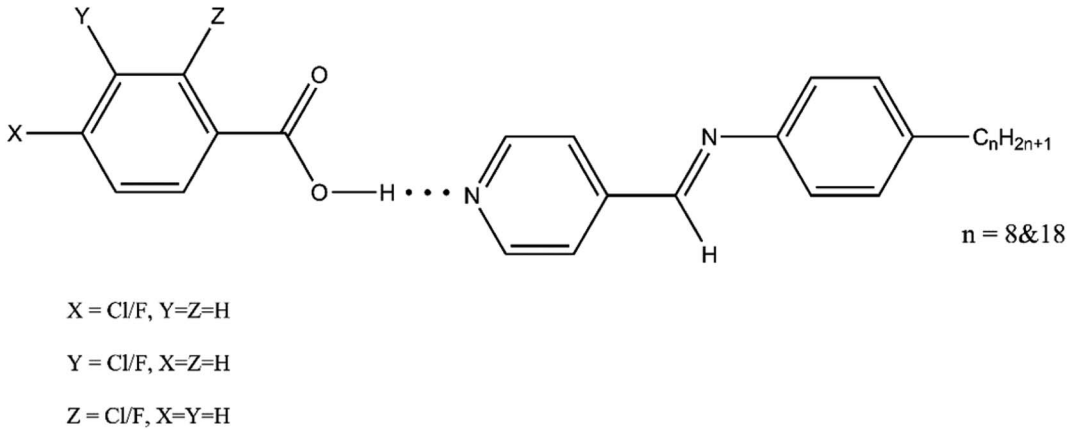

Fig. 1 Molecular structure of the HBLCs.

benzoic acids. Our investigation considers the mesomorphic behaviour, dipole moment, enthalpy changes and polarity, while also examining the effect of size of benzoic acid substituents. The study provides well-defined theoretical interpretations and precise experimental results, offering valuable ideas for future material design.

2. Materials and methods

Benzoic acids, including *o*-chlorobenzoic acid (2ClBA), *m*-chlorobenzoic acid (3ClBA), *p*-chlorobenzoic acid (4ClBA), *o*-fluorobenzoic acid (2FBA), *m*-fluorobenzoic acid (3FBA) and *p*-fluoro benzoic acid (4FBA) are purchased from MERCK India and Sigma-Aldrich. Intermolecular hydrogen bonding is verified through IR spectral analysis using Shimadzu 00254 and the ATR probing method. The liquid crystal mesophases are studied using the Polarizing Optical Microscopy (POM) instrument Leitz DMRXP Polarizing Optical Microscope (POM) with METTLER HS1 hot stage controller and instrument SDTECHS-model no. SDVPM 2727 with a cooling rate of 2 °C min^{-1}. Differential scanning calorimetry was done with a Shimadzu DSC60 instrument, and samples were crimped in weighted aluminum pans (~2 mg).

2.1. Theoretical

The DFT method utilizing wb97x-D theory along with the cc-pVTZ basis set were used for the calculations. The use of wb97x-D theory is more suited for calculations involving non-covalent interactions. All the geometry optimization calculation was followed by harmonic frequency calculation to ensure the optimized structure at the global minimum of the potential energy surface. All the calculations were performed using Gaussian09 (Rev. D) program package.

The hybrid functional B3LYP-D3 and Gaussian type basis set 6-31G(d,p) were used for studying the orientation of the molecules.

2.2. Experimental

2.2.1. Synthesis of proton acceptor and preparation of HBLCs. Our previous work summarized the formation of supramolecular compounds using (4-pyridyl)-benzylidene-4′-*n*-octyl aniline (P8) as a proton acceptor and 2ClBA, 3ClBA and 4ClBA as proton donors, and the study of their mesophase behavior.[21] The second series of HBLCs are prepared with already synthesized (4-pyridyl)-benzylidene-4′-*n*-octadecyl aniline (P18) as a proton acceptor where a 1 : 1 ratio of 4-pyridine carboxaldehyde and 4-*n*-octadecyl aniline is refluxed in ethanol for 7 hours to obtain P18. The P18 is hydrogen bonded to 2ClBA, 3ClBA and 4ClBA as proton donors. The mesomorphic behavior of the HBLCs of P18 is discussed in the current paper, and the effect of the substituent size is described (Fig. 1).

3. Results and discussion

3.1. Fourier transform infra-red (FTIR) spectroscopy

FTIR measurements are carried out on synthesized compounds and the obtained plots are baseline corrected. The narrowing of the O–H stretching peak at 3070–2542 cm^{-1} to 2916 cm^{-1} in

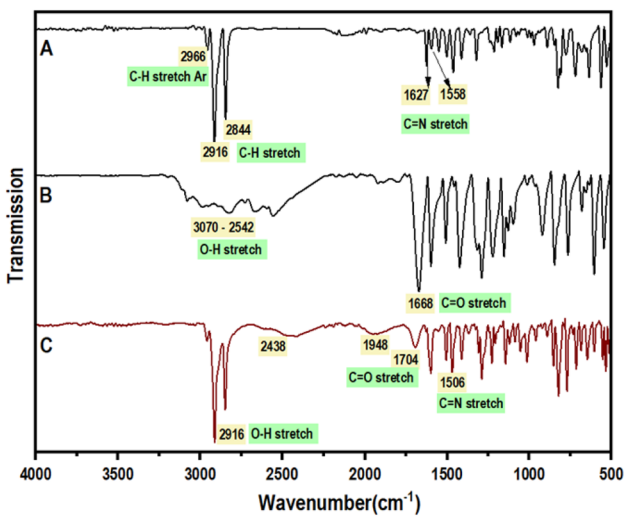

Fig. 2 Comparative FTIR spectrum of, (A) (4-pyridyl)-benzylidene-4′-*n*-octadecylaniline (P18) (B) 4-fluorobenzoic acid (4FBA) (C) HBLC, P18:4FBA.

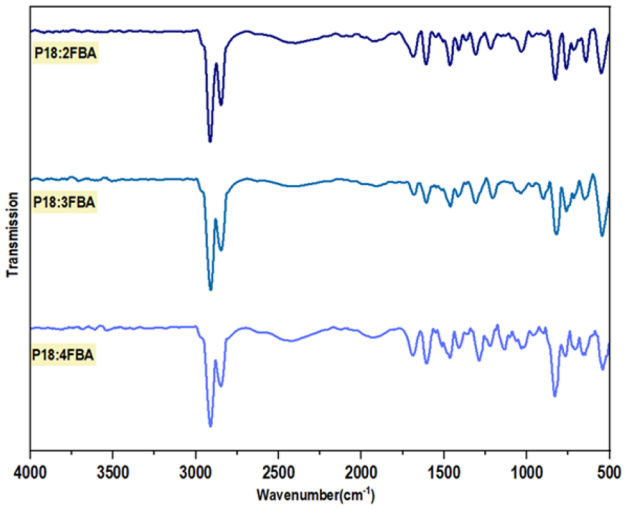

Compound	$\bar{\upsilon}_{O-H}$ (Cm^{-1})	$\bar{\upsilon}_{C=O}$ (Cm^{-1})	$\bar{\upsilon}_{C=N}$ (Cm^{-1})	$\bar{\upsilon}_{HB}$ (Cm^{-1})
P18:2FBA	2914	1696	1611	2424 1930
P18:3FBA	2916	1701	1612	2428 1969
P18:4FBA	2916	1704	1608	2438 1948

Fig. 3 Comparative FTIR spectrum of P18:2FBA, P18:3FBA and P18:4FBA.

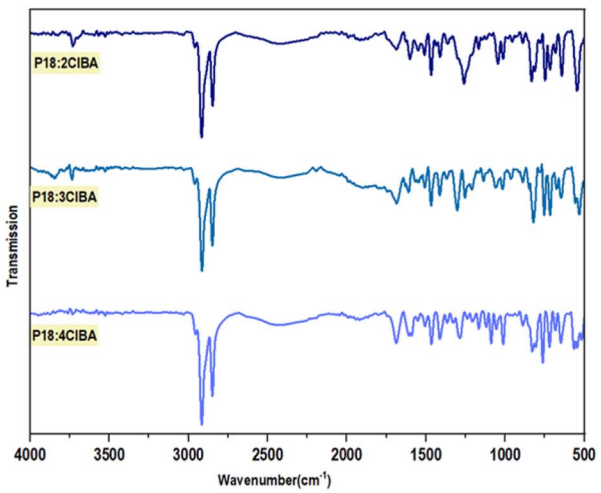

Compound	$\bar{\upsilon}_{O-H}$ (Cm^{-1})	$\bar{\upsilon}_{C=O}$ (Cm^{-1})	$\bar{\upsilon}_{C=N}$ (Cm^{-1})	$\bar{\upsilon}_{HB}$ (Cm^{-1})
P18:2ClBA	2917	1695	1602	2441 1950
P18:3ClBA	2917	1688	1608	2434 1945
P18:4ClBA	2919	1689	1604	2458 1943

Fig. 4 Comparative FTIR spectrum of P18:2ClBA, P18:3ClBA and P18:4ClBA.

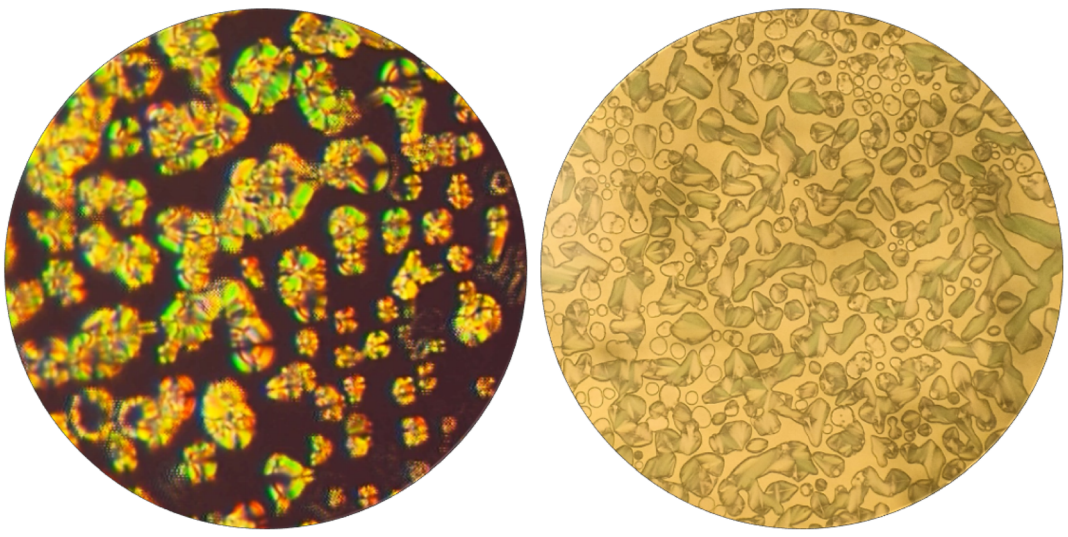

Fig. 5 Smectic A mesophases exhibited by (a) P18:4FBA (10×) (b) P18:4ClBA (10×).

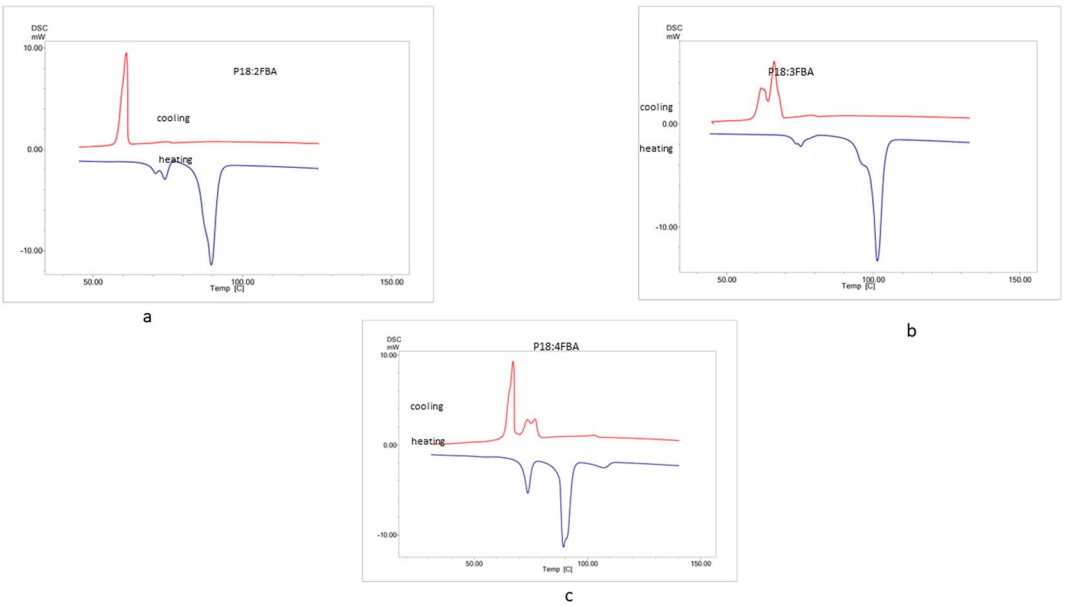

Fig. 6 DSC thermograms for the HBLC's: (a) P18:2FBA; (b) P18:3FBA; (c) P18:4FBA.

4FBA reveals the complementary nature of acids transforming into linear structures when forming intermolecular hydrogen bonds (Fig. 2).[22] Peaks at 2438 cm^{-1} and 1948 cm^{-1} indicate new hydrogen bonding interactions of P18. The C=O of the acid and C=N stretch of the Schiff base is observed at 1704 and 1608 cm^{-1} respectively. Tabulated characteristic peaks for the O–H stretching of the acid, C=O stretching of the carboxyl group, and C=N stretching of the Schiff base are presented for the clubbed FTIR spectra of P18:2FBA, P18:3FBA, P18:4FBA (Fig. 3) and P18:2ClBA, P18:3ClBA, and P18:4ClBA (Fig. 4).

3.2. Phase transition studies by polarizing optical microscopy (POM)

The polarizing optical microscopy images of *ortho*, *meta*, and *para*-substituted hydrogen bonded compounds of P18 exhibited orthogonal smectic A mesophases. Initially, small bubble-like structures were observed, which grew into bonnet-like structures and eventually formed beautiful, focal conic textures. Same observations are made by the P8 hydrogen bonded analogs wherein the confirmation of smectic A mesophase is carried out by temperature variation XRD (Fig. 5).[21] The POM

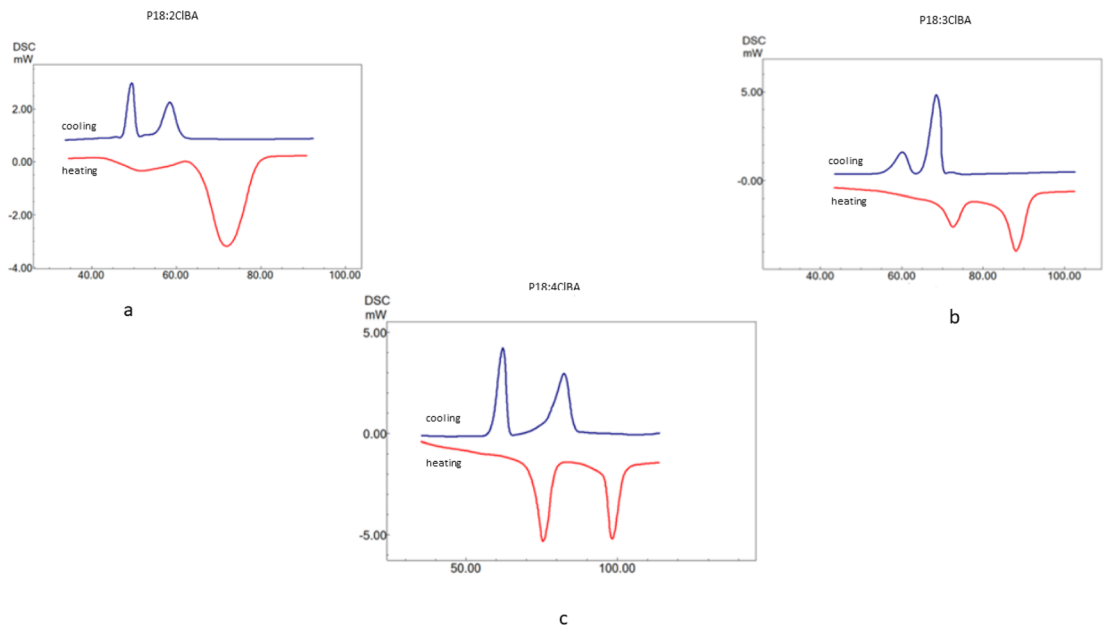

Fig. 7 DSC thermograms for the HBLC's: (a) P18:2ClBA; (b) P18:3ClBA; (c) P18:4ClBA.

Table 1 DSC phase transition temperature (°C) and the corresponding enthalpy (J g^{-1}) of P18 with fluorobenzoic acids[a]

Hydrogen bonded compound	Method	Transition	Transition temperatures (°C) (enthalpy J g^{-1})	$(\Delta T)_{LC}$
PyB18A:2FBA	DSC (h)	Cryst → SmA	72.0 (4.57)	
		SmA → Iso	89.45 (83.45)	
	DSC (c)	Iso → SmA	74.26 (1.50)	13.24
		SmA → Cryst	61.02 (68.67)	
PyB18A:3FBA	DSC (h)	Cryst → SmA	74.06 (5.06)	
		SmA → Iso	101.41 (58.58)	
	DSC (c)	Iso → SmA	78.78 (1.72)	12.79
		SmA → $Cryst^1$	65.99 (34.15)	
		Crystl → $Cryst^2$	61.92 (6.04)	
PyB18A:4FBA	DSC (h)	$Cryst^1$ → $Cryst^2$	73.53 (20.22)	
		$Cryst^2$ → SmA	89.58 (73.03)	
		SmA → Iso	107.36 (5.93)	
	DSC (c)	Iso → SmA	103.33 (1.86)	28.02
		SmA → $Cryst^1$	75.31(26.88)	
		$Cryst^1$ → $Cryst^2$	67.03 (64.09)	

[a] DSC (h) is heating cycle, DSC (c) is cooling cycle. $(\Delta T)_{LC}$ is the thermal range of mesomorphism obtained from the cooling cycle.

Table 2 DSC phase transition temperature (°C) and the corresponding enthalpy (J g^{-1}) of P18 with chlorobenzoic acids

Hydrogen bonded compound	Method	Transition	Transition temperatures (°C) (enthalpy J g^{-1})	$(\Delta T)_{LC}$
PyB18A:2ClBA	DSC (h)	Cryst → SmA	51.27 (13.88)	
		SmA → Iso	71.68 (84.68)	
	DSC (c)	Iso → SmA	58.38 (21.57)	9.02
		SmA → Cryst	49.36 (29.04)	
PyB18A:3ClBA	DSC (h)	Cryst → SmA	72.75 (18.40)	
		SmA → Iso	87.95 (40.19)	
	DSC (c)	Iso → SmA	68.69 (53.48)	9.13
		SmA → Cryst	59.56 (23.20)	
PyB18A:4ClBA	DSC (h)	Cryst → SmA	75.46 (36.78)	
		SmA → Iso	98.57(28.61)	
	DSC (c)	Iso → SmA	82.16 (29.29)	20.06
		SmA → Cryst	62.10 (52.71)	

Table 3 DSC phase transition temperature (°C) and the corresponding enthalpy (J g^{-1}) of P8 with fluoro and chlorobenzoic acids

Hydrogen bonded compound	Method	Transition	Transition temperatures (°C) (enthalpy J g^{-1})	$(\Delta T)_{LC}$
PyB8A:2FBA	DSC (h)	Cryst → Iso	66.42 (50.09)	
	DSC (c)	Iso → SmA	53.69 (1.61)	25.64
		SmA → Cryst	28.05 (26.61)	
PyB8A:3FBA	DSC (h)	Cryst → Iso	91.52 (59.96)	
	DSC (c)	Iso → SmA	69.08 (3.34)	25.14
		SmA → Cryst	43.94 (51.45)	
PyB8A:4FBA	DSC (h)	Cryst → SmA	61.44 (40.49)	
		SmA → Iso	[a]	
	DSC (c)	Iso → SmA	99.71 (6.09)	56.57
		SmA → Cryst	43.14(41.65)	
PyB8A:3ClBA	DSC (h)	Cryst → Iso	72.00(51.88)	
	DSC (c)	Iso → SMA	66.03 (5.86)	12.84
		SmA → Cryst	53.19(48.92)	
PyB8A:4ClBA	DSC (h)	Cryst → SmA	91.73 (35.04)	
		SmA → Iso	117.26 (6.34)	
	DSC (c)	Iso → SmA	109.57 (2.55)	52.42
		SmA → Cryst	57.15(20.28)	

[a] Not resolved.

Table 4 Comparison of mesomorphic thermal stability

Compound	2ClBA	2FBA	3ClBA	3FBA	4ClBA	4FBA
P8	[a]	25.64	12.84	25.14	52.42	56.57
P18	9.02	13.24	9.13	12.79	20.06	28.02

[a] Liquid at RT.

images of P8 compounds are included in the ESI as Fig. S1 and S2.†

3.3. Thermal characterization by differential scanning calorimetry (DSC)

The thermal range of mesomorphism confirmed by differential scanning calorimetry carried under nitrogen atmosphere is summarized (Fig. 6 and 7). Tables 1–3 summarizes the phase transition temperature (°C) where transition from crystal to SmA to isotropic state is observed in the heating cycle and isotropic to SmA to crystal is observed in the cooling cycle. The change in enthalpy accompanying the phase transition is also summarized in the table.

The observations are summarized as follows:

(i) Liquid crystalline behaviour of the hydrogen bonded compounds of P8 and P18 based on the position of the substituent:

It can be observed that the hydrogen bonded compounds between the proton acceptors (P8, P18) and *x*-chloro/fluorobenzoic acids (*x*ClBA/*x*FBA, *x* represents the position of chloro/fluoro substituent at benzene) show that the trend of variation in mesomorphic thermal stabilities of fluoro substituted benzoic acid compounds are in the order *para* > *ortho* > *meta*. In contrast, chloro-substituted benzoic acid complexes are following *para* > *meta* in P8:hydrogen bonded compounds and *para* > *ortho* ≈ *meta* in P18:hydrogen bonded compounds (Table 4) and (Fig. 8).

Hydrogen bonded compounds of fluoro-substituted acids show that the *para* isomers, P8/18:4FBAs, have the highest mesomorphic thermal stability than the other two isomers (*ortho* and *meta*) for a given proton acceptor moiety. This may be attributed to enhancing the length-to-breadth ratio and higher longitudinal dipole moment (along the long molecular axis) of the compounds. When the fluorine is in *ortho* position to the carbonyl group of carboxylic acid, the high charge density of fluorine (due to its small size) repels the similarly charged oxygen atom of the carbonyl group.[23] This leads to the reduction of co-planarity between the carbonyl moiety and the phenyl ring to which it is attached, thus resulting in a lower mesomorphic thermal stability. Contrary to the expected higher mesomorphic thermal stability of 3FBA complexes (P8/18:3FBA) compared to 2FBA complexes, they are exhibiting the lowest mesomorphic thermal stability despite their co-planarity (as the fluorine is oriented away from the carbonyl group). It may be due to the molecular broadening effect due to the decrease in the HB complex's geometrical anisotropy (*i.e.*, less *l*/*b*).[24] These results agree with the report on non-HBLCs, in which the effect of rigid core and position of fluorine on thermal stability is studied.[25] Comparison of the clearing and melting temperatures of the newly synthesized compounds (Fig. 9) reveals that chlorine substituted hydrogen bonded compounds are exhibiting lower clearing and melting temperatures as compared to fluorine substituted hydrogen bonded compounds. This may be

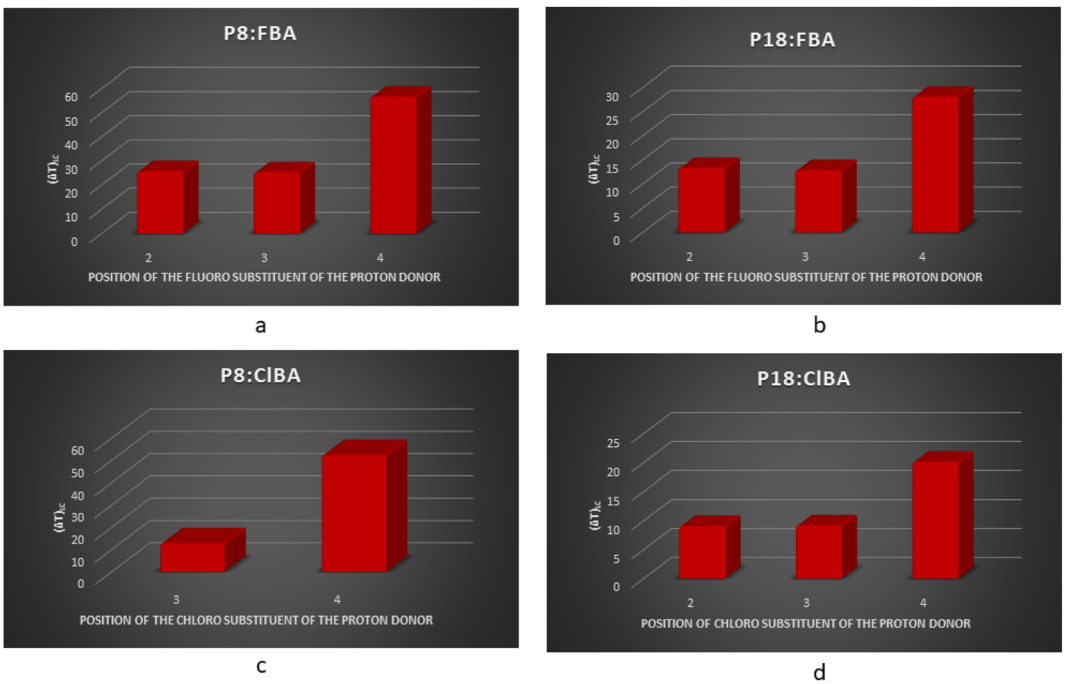

Fig. 8 Bar diagrams comparing the mesomorphic thermal stabilities of *ortho*, *meta* and *para* substituted benzoic acids hydrogen bonded with P8 and P18: (a) P8:FBA; (b) P18:FBA; (c) P8:ClBA; and (d) P18:ClBA.

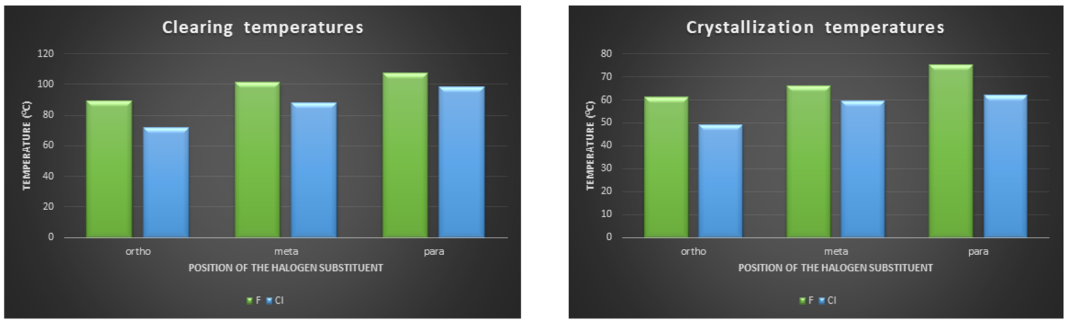

a b

Fig. 9 Bar diagrams comparing the (a) clearing and (b) crystallization temperatures of fluoro and chloro substituted hydrogen bonded compounds of P18.

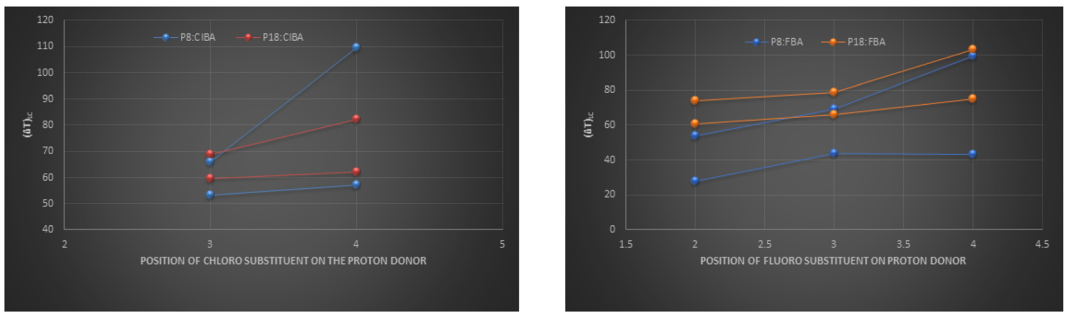

Fig. 10 Comparison of mesomorphic thermal range of fluoro-substituted hydrogen-bonded compounds of P8 and P18 with chloro-substituted hydrogen bonded compounds.

attributed to the bigger size of the chlorine atoms leading to the decreased co-planarity between molecular chains and thus leading to the decreased intermolecular forces. The decreased intermolecular interactions thus lead to the decreased clearing and melting temperatures. This result agrees with the work done by Maher *et al.*.[26]

(ii) Comparison of fluoro substituted hydrogen bonded compounds of P8 and P18 with chloro substituted hydrogen bonded compounds.

The P8:*x*FBA compounds exhibit a higher mesomorphic thermal stability than the corresponding P18:*x*FBA compounds, and P8:*x*ClBA compounds exhibit a higher mesomorphic thermal stability than the corresponding P18:*x*ClBA compounds (Fig. 10).

The higher mesomorphic thermal stability of P8:*x*FBA compounds is attributed to the highly polar C–F bond (due to the high electronegativity of fluorine), which enhances the intermolecular interactions with neighboring molecules, leading to a higher smectic thermal stability. At the same time, the bulky and less electronegative (compared to fluorine) chlorine atom pushes the molecules apart due to steric hindrance. It decreases the net intermolecular interactions among the different moieties, resulting in lower mesomorphic thermal stability. This observation is concurrent with the report on non-HBLCs, in which the 3-fluoro substituted esters exhibit higher mesomorphic stabilities than the corresponding 3-chloro substituted esters.[27] With the increase in the chain

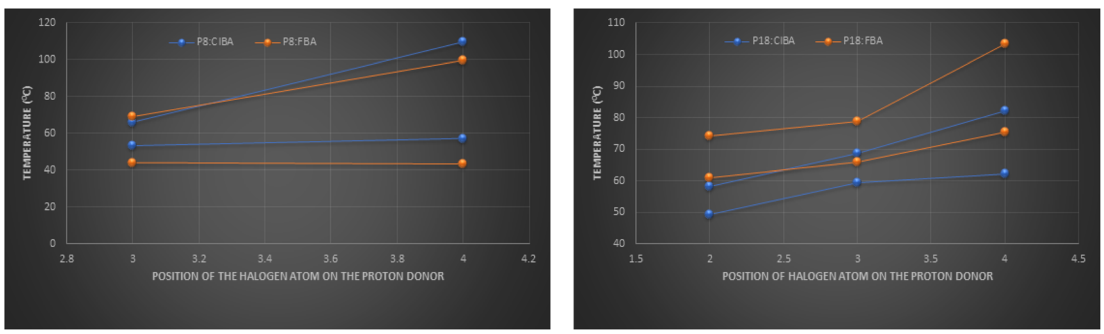

Fig. 11 Comparison of mesomorphic thermal range of fluoro and chloro substituted hydrogen bonded compounds of P8 and P18.

Table 5 Ionization energy, electron affinity and size of chlorine and fluorine atoms

Substituent	IE (kJ mol^{-1})	EA(1) (kJ mol^{-1})	Size (pm)
Fluorine	1681	−328	72
Chlorine	1258	−349	100

length of the proton acceptor, a dilution of the core is envisaged. This leads to the decrease in the mesomorphic thermal behaviour with the increased chain length. In the case of P18:*x*ClBA complexes, the bulky chlorine atoms compensate for the core's dilution caused by the proton acceptor's flexible alkyl end chain.

(iii) Comparison of fluoro and chloro-substituted hydrogen bonded compounds of P8 with fluoro and chloro-substituted hydrogen bonded compounds of P18.

It is observed that P8:*x*FBA compounds are exhibiting higher mesomorphic behavior as compared to P8:*x*ClBA compounds, and P18:*x*FBA are exhibiting higher mesomorphic behavior as compared to P18:*x*ClBA compounds (Fig. 11).

As the fundamental goes, similar outer electron configurations correlate with similar chemical behavior. Fluorine and chlorine have condensed electron configuration [noble gas] ns^2np^5. With the increase in the principal quantum number (n), the probability that the outer electrons will spend more time farther from the nucleus increases, making the atoms larger. This makes the atomic radii of fluorine as 72 pm and chlorine as 100 pm. The ionization energy of fluorine is 1681 kJ mol^{-1}, and that of chlorine is 1258 kJ mol^{-1}. The first electron affinity of fluorine is −328 kJ mol^{-1}, while that of chlorine is −349 kJ mol^{-1}. The high ionization energies and highly negative (exothermic) electron affinities of fluorine and chlorine make them highly reactive non-metals, as summarized below in Table 5.[28]

Comparing the proton donors like chloro benzoic acids with fluoro benzoic acids, it is evident that chloro benzoic acids have stronger electron donating ability than the fluoro substituted acids while they match the electron-withdrawing abilities with a minor difference. Considering the size as a parameter, it may be argued that the small size of the fluorine atom holds its valence electrons tightly to the nucleus, making it less polarizable compared to the chlorine atom. On the other hand, the chlorine atom is larger than the fluorine atom and hence gets polarized easily as the valence electrons on this are far away from the nucleus. It is reported by Guan Yeow Yeap *et al.* that the molecular ordering increases as the polarizability of the compound increases.[24] It is observed that in our present study, fluoro-substituted P8:hydrogen bonded compounds exhibit a larger mesomorphic range as compared to chloro-substituted P8:hydrogen bonded compounds. Although the higher polarizable chlorine atoms of the benzoic acids do favor molecular ordering, the size dominates and pushes the molecules apart and reduces the mesophase stability. Similarly with the increase in the chain length of proton acceptor from P8 to P18, fluoro substituted P18:hydrogen bonded compounds exhibit a higher range of mesomorphism as compared to chloro substituted P18:hydrogen bonded compounds. An increase in chain length leads to the dilution of the core.[29,30] Do the bulky chlorine atoms compensate for the core's dilution caused by the proton acceptor's flexible alkyl end chain? As reported by Yeap G. Y. *et al.* the terminal substituents' volume and the terminal substituted atoms' radius influence phase transitions.[31] The terminal substituents with large volume, large radius, and high branching degree are found to be more polarized. They are conducive to filling the space effectively and thus helpful in improving thermal stability and mesomorphic behavior.

3.4. Theoretical simulation

A simulation study is carried out on the hydrogen bonded compounds supporting the above observations. The molecules are optimized, the parallel and anti-parallel orientation is obtained, the free volume calculations are performed by employing the Schrödinger python module of free volume calculator as included in the Material Science suit of packages. Fig. 12 shows the optimized structure of molecular compounds using the Gaussian program package. Optimization was performed using wb97x-D

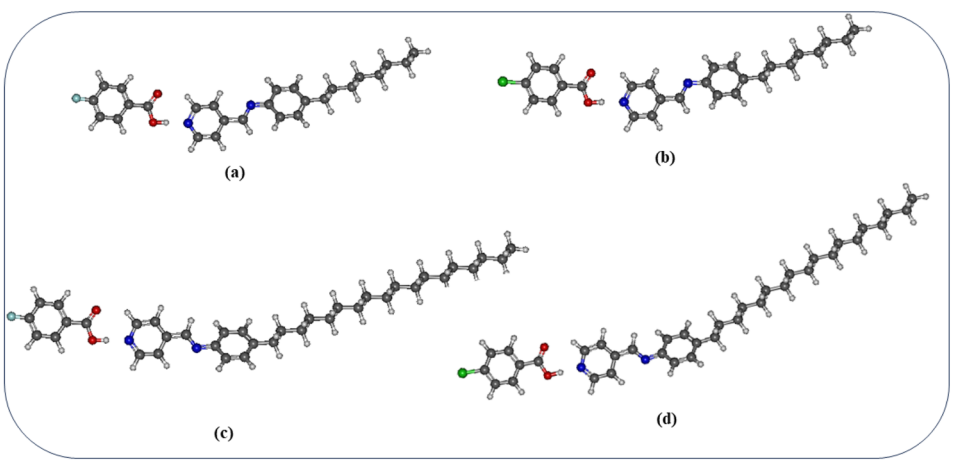

Fig. 12 Optimized structures of molecular compounds (a) P8:4FBA; (b) P8:4ClBA; (c) P18:4FBA; (d) P18:4ClBA.

Table 6 The dipole moment and polarizability of P8 and P18 hydrogen bonded compounds

Hydrogen bonded compounds	OH–N (Å)	O–HC (Å)	Dipole moment (μ) (debye)	Polarizability (α) (a.u.)
P8:4ClBA	1.7155	2.4023	6.71	372.99
P8:4FBA	1.7206	2.4024	6.20	357.46
P18:4ClBA	1.7165	2.3534	5.96	497.04
P18:4FBA	1.7255	2.3390	5.40	482.14

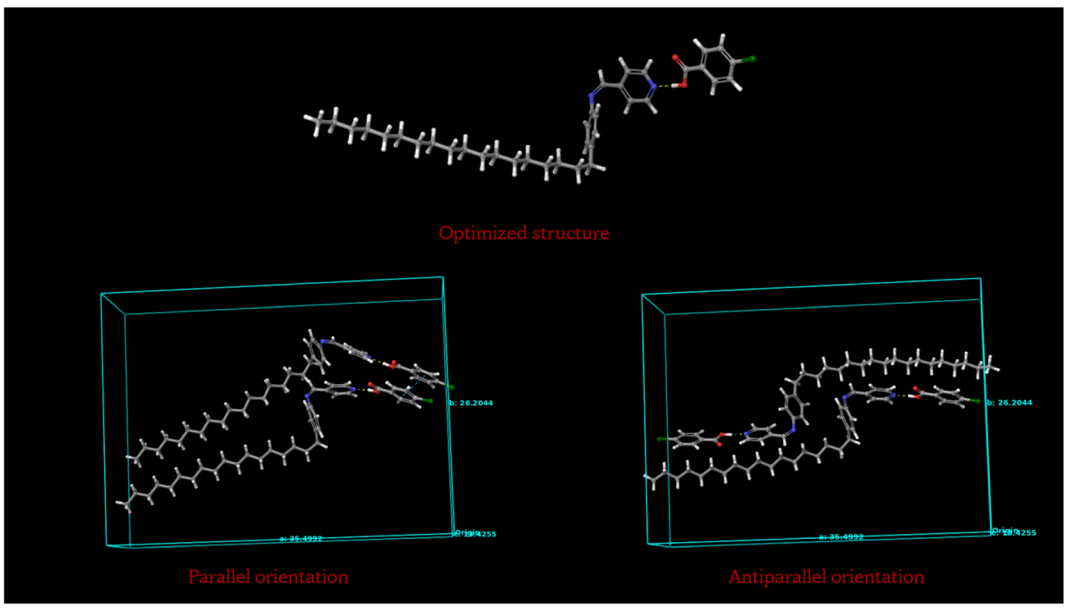

Fig. 13 Optimized structure of P18:4ClBA, parallel and anti-parallel orientation of molecules.

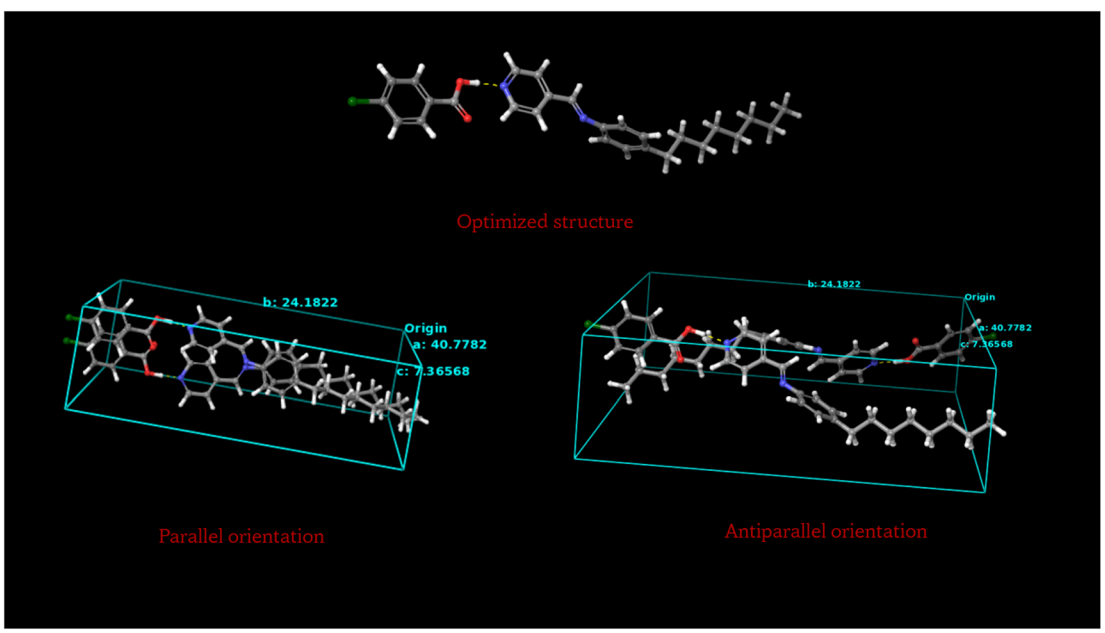

Fig. 14 Optimized structure of P8:4ClBA, parallel and anti-parallel orientation of molecules.

Table 7 The orientation and free volume of hydrogen bonded compounds

Hydrogen bonded compounds	Orientation	Total energy (kcal mol^{-1})	Free volume (%)
P18:4CIBA	Parallel	-2712.15×10^3	72.89
P18:4CIBA	Anti-parallel	-2712.16×10^3	73.84
P8:4CIBA	Parallel	-2218.70×10^3	73.17
P8:4CIBA	Anti-parallel	-2218.30×10^3	65.31
P18:4FBA	Parallel	-2259.89×10^3	73.27
P18:4FBA	Anti-parallel	-2259.91×10^3	74.56
P8:4FBA	Parallel	-1765.92×10^3	70.66
P8:4FBA	Anti-parallel	-1765.93×10^3	72.24

theory level and cc-pVTZ basis set using Gaussian 09 program package.[32,33] As shown in Fig. 12, the compound is stabilized by two hydrogen bonds between benzoic acid and pyridine rings of molecules. The hydrogen bond lengths of four compounds are listed in Table 6, along with their dipole moments.

Fig. 13 shows the optimized structure of P18:4ClBA, the parallel and anti-parallel orientation of the molecules. Fig. 14 shows the optimized structure of P8:4ClBA, the parallel and anti-parallel orientation of the molecules. Similarly P18:FBA and P8:FBA compounds are checked for molecular orientation.

The total energy exhibited by parallel and anti-parallel alignment of P18:4ClBA molecules are -2712.15×10^3 kcal mol^{-1} and -2712.16×10^3 kcal mol^{-1} respectively while parallel and anti-parallel alignment of P8:4ClBA molecules are -2218.70×10^3 kcal mol^{-1} and -2218.30×10^3 kcal mol^{-1} respectively. The free volume calculated for parallel orientation of P18:4ClBA molecules is found to be 72.89% while that of P8:4ClBA is 73.17%. Similarly for parallel orientation of P18:4FBA molecules, the energy is -2259.89×10^3 kcal mol^{-1} and free volume is 73.27% while that of P8:4FBA molecules the energy is -1765.92×10^3 kcal mol^{-1} and free volume is 70.66%. The data pertaining to the same is summarized in Table 7.

It may be observed that as the chain length increases, the free volume is increasing indicating the dilution of the core caused by the longer chain lengths leading to less orderly packed molecules. On the other hand, for similar chain lengths, fluoro substituted compounds are exhibiting more free volume compared to chloro substituted compounds. From this observation, it may be inferred that the bigger size of the substituent helps better stack the molecules by compensating for the dilution of the core caused by longer terminal chain lengths.

4. Conclusion

New hydrogen bonded compounds are successfully synthesized, and the mesomorphic behavior is analyzed. The size of the substituent is found to influence the mesomorphism. *Para* substituted H-bonded compounds exhibit the highest mesomorphic thermal behavior due to enhanced length-to-breadth ratio and higher longitudinal dipole moment (along the long molecular axis) of the compounds. *Ortho* substituents lead to the reduction of co-planarity between the carbonyl moiety and the phenyl ring to which it is attached, thus resulting in a lower mesomorphic thermal stability. The lower mesomorphic thermal stabilities of *meta* substituted compounds are due to the molecular broadening effect due to the decrease in the HB complex's geometrical anisotropy (*i.e.*, less *l*/*b*). The higher mesomorphic thermal stability of fluorine containing compounds is attributed to the highly polar C–F bond (due to the high electronegativity of fluorine), which enhances the intermolecular interactions with neighboring molecules while the bulky chlorine atom due to steric hindrance results in lower mesomorphic thermal stability. With a crystallization temperature of 49.36 °C, P18:2ClBA exhibits ambient mesomorphic behaviour. When the size of the substituent is significant, better stacking is envisioned with molecules possessing longer chain lengths.

Data availability

The data supporting this article have been included as part of the ESI.

Author contributions

Conceptualization-Poornima Bhagavath. Methodology-Poornima Bhagavath & Sonali M. K. Formal analysis-Poornima Bhagavath, Sonali M. K. & Rajeev K. Sinha. Investigation-Sonali M. K., Silpa Elizabeth, Anil Kumar N. V., Nirmal Mazumder, Sindhoora Kaniyala Melanthota, Mohammed Azeezulla Nazrulla. Writing – original draft-Poornima Bhagavath, Sonali M. K. & Rajeev K. Sinha. Writing – review & editing-Poornima Bhagavath, Sonali M. K. and Rajeev K. Sinha. Funding acquisition-Poornima Bhagavath. Resources-Poornima Bhagavath. Supervision-Poornima Bhagavath.

Conflicts of interest

There are no conflicts to declare.

Acknowledgements

We thank Dr Srinivasulu Maddasani, Associate Professor (Senior Scale) at the Department of Chemistry, MIT, Manipal, for his guidance and support. We thank the Centre for Nano and Soft Matter Sciences (CeNS) Bengaluru for providing advanced liquid crystal characterization resources. NM thank

the Department of Biotechnology (DBT), Government of India, (project number: BT/PR25099/NER/95/1014/2017). Intramural grants from the Manipal Academy of Higher Education have enabled us to pursue research with renewed vigor.

References

1 T. Kato and J. M. J. Fréchet, Stabilization of a Liquid-Crystalline Phase through Noncovalent Interaction with a Polymer Side Chain, *Macromolecules*, 1989, **22**, 3818–3819, DOI: 10.1021/ma00199a060.

2 T. Kato, H. Kihara, T. Yu, S. Ujiie, K. Iimura, J. M. J. Fréchet and U. Kumar, Hydrogen-bonded ferroelectric liquid-crystalline complexes based on a chiral benzoic acid and stilbazoles. Induction of chiral smectic C phases by molecular self-assembly, *Ferroelectrics*, 1993, **148**, 161–167, DOI: 10.1080/00150199308019942.

3 L. J. Yu, Hydrogen bond-induced ferroelectric liquid crystals, *Liq. Cryst.*, 1993, **14**, 1303–1309, DOI: 10.1080/02678299308026443.

4 T. Kato, H. Kihara, U. Kumar, T. Uryu and J. M. J. Frechet, A Liquid-Crystalline Polymer Network Built by Molecular Self-Assembly through Intermolecular Hydrogen Bonding, *Angew. Chem., Int. Ed. Engl.*, 1994, **33**, 1644–1645, DOI: 10.1002/anie.199416441.

5 T. Kato, M. Fukumasa and J. M. J. Fréchet, Supramolecular Liquid-Crystalline Complexes Exhibiting Room-Temperature Mesophases and Electrooptic Effects. Hydrogen-Bonded Mesogens Derived from Alkylpyridines and Benzoic Acids, *Chem. Mater.*, 1995, **7**, 368–372, DOI: 10.1021/cm00050a021.

6 K. Willis, D. J. Price, H. Adams, G. Ungar and D. W. Bruce, Hydrogen-bonded liquid crystals from alkoxystilbazoles and 3-cyanophenols: structural control of mesomorphism. Molecular structure of the complex between 4-cyanophenol and 4-octyloxystilbazole, *J. Mater. Chem.*, 1995, **5**, 2195–2199, DOI: 10.1039/jm9950502195.

7 T. Kato, Supramolecular liquid crystalline materials: molecular self assembly and self-organization through intermolecular hydrogen bonding, *Supramol. Sci.*, 1996, **3**, 53–59, DOI: 10.1016/0968-5677(96)00026-0.

8 M. Muniprasad, M. Srinivasulu, P. V. Chalapathi and D. M. Potukuchi, Influence of chemical moieties and the flexible chain for the tilted smectic phases in linear hydrogen bonded liquid crystals with Schiff-based pyridine derivatives, *J. Mol. Struct.*, 2012, **1015**, 181–191, DOI: 10.1016/j.molstruc.2011.10.007.

9 C. M. Paleos and D. Tsiourvas, Thermotropic Liquid Crystals Formed by Intermolecular Hydrogen Bonding Interactions, *Angew. Chem., Int. Ed. Engl.*, 1995, **34**, 1696–1711, DOI: 10.1002/anie.199516961.

10 C. M. Paleos and D. Tsiourvas, Supramolecular hydrogen-bonded liquid crystals, *Liq. Cryst.*, 2001, **28**, 1127–1161, DOI: 10.1080/02678290110039516.

11 T. Missaoui, I. B. Amor, T. Soltani, H. B. Ouada, E. Jeanneau and Y. Chevalier, Dielectric and electro-optic properties of cybotactic nematic phase in hydrogen-bonded liquid crystals, *J. Mol. Liq.*, 2020, **304**, 112726, DOI: 10.1016/j.molliq.2020.112726.

12 P. Bhagavath, S. G. Bhat, S. Mahabaleshwara, S. R. Girish, D. M. Potukuchi, P. V. Chalapathi and M. Srinivasulu, Mesomorphic thermal stabilities in supramolecular liquid crystals: influence of the size and position of a substituent, *J. Mol. Liq.*, 2013, **186**, 56–62, DOI: 10.1016/j.molliq.2013.05.013.

13 M. Srinivasulu, P. V. V. Satyanarayana, P. A. Kumar and V. G. K. M. Pisipati, Induced Smectic-G phase through Intermolecular Hydrogen Bonding Part V-Thermal and Crystallization Kinetics Studies, *Mol. Mater.*, 2001, **14**, 215–232.

14 P. A. Kumar, M. Srinivasulu and V. G. K. M. Pisipati, Induced smectic G phase through intermolecular hydrogen bonding, *Liq. Cryst.*, 1999, **26**(9), 1339–1343, DOI: 10.1080/026782999204002.

15 S. G. Bhat, M. Srinivasulu, S. R. Girish, P. Bhagavath, S. Mahabaleshwara, D. M. Potukuchi and M. Muniprasad, Influence of Moieties and Chain Length on the Abundance of Orthogonal and Tilted Phases of Linear Hydrogen-Bonded Liquid Crystals, Py16BA:nOBAs, *Mol. Cryst. Liq. Cryst.*, 2012, **552**, 83–96, DOI: 10.1080/15421406.2011.604569.

16 M. Fouzai, A. Guesmi, N. ben Hamadi and T. Soltani, Fluoro-substitution in hydrogen bonding liquid crystal benzoic acid: dielectric, electro-optic and optical proprieties and inducing polar nematic phase, *Liq. Cryst.*, 2020, **47**(5), 777–784, DOI: 10.1080/02678292.2019.1679900.

17 B. Meddeb, A. Gesmi, N. ben Hamadi and T. Soltani, Enhancement of thermal, dielectric and electro-optical properties of fluoro hydrogen-bonded liquid crystals, *Liq. Cryst.*, 2021, **48**, 1175–1185, DOI: 10.1080/02678292.2020.1850895.

18 M. Fouzai, P. Dieudonné-George, A. Guesmi, N. B. Hamadi, Y. Arfaoui, T. Soltani and Y. Chevalier, Polar nematic phase in short-chained fluorinated hydrogen-bonded liquid crystals, *J. Mol. Liq.*, 2023, **375**, 121307, DOI: 10.1016/j.molliq.2023.121307.

19 M. Derbali, T. Soltani, A. Guesmi, N. B. Hamadi, E. Jeanneau and Y. Chevalier, Synthesis, Thermal, Dielectric and Electro-Optic Properties of New Series of Fluorinated Hydrogen-Bonded Liquid Crystals, *J. Mol. Liq.*, 2022, **367**, 120510.

20 O. D. Johnson, S. G. Wainwright, A. C. Whitwood and D. W. Bruce, Hydrogen-bonded liquid crystals formed from 4-alkoxystilbazoles and chlorophenols, *CrystEngComm*, 2023, **25**, 2778–2788, DOI: 10.1039/D3CE00266G.

21 M. K. Sonali, P. Bhagavath, M. Srinivasulu, R. K. Sinha and K. Swamynathan, Induced mesomorphism in supramolecular structures of H-bonded binary mixtures containing fluoro and chloro substituted benzoic acids, *J. Fluorine Chem.*, 2022, **259–260**, 110002, DOI: 10.1016/j.jfluchem.2022.110002.

22 R. M. Silverstein, F. X. Webster and D. J. Kimley, *Spectrometric Identification of Organic Compounds*, John Wiley & Sons Inc, New Jersey, 7th edn, 2005.

23 G. W. Gray, C. Hogg and D. Lacey, The synthesis and liquid crystal properties of some laterally fluorinated trans-cyclohexane-1-carboxylate and benzoate esters, *Mol. Cryst. Liq. Cryst.*, 1981, **67**, 1–23, DOI: **10.1080/00268948108070871**.

24 G. Y. Yeap, S. T. Ha, P. Lim, P. Boey, M. M. Ito, S. Sanehisa and Y. Youhei, Synthesis, physical and mesomorphic properties of Schiff's base esters containing *ortho* -, *meta*- and *para*- substituents in benzylidene-4′-alkanoyloxyanilines, *Liq. Cryst.*, 2006, **33**, 205–211, DOI: **10.1080/02678290500450584**.

25 M. M. Naoum, A. A. Fahmi and W. A. Almllal, Supramolecular liquid crystals induced by hydrogen bonding interactions between non-mesogenic compounds II. Effect of lateral substitution, *Mol. Cryst. Liq. Cryst.*, 2010, **518**, 109–128, DOI: **10.1080/15421400903568070**.

26 M. A. Qaddoura and K. D. Belfield, Synthesis, Characterization and Texture Observations of Calamitic Liquid Crystalline Compounds, *Int. J. Mol. Sci.*, 2009, **10**, 4772–4788, DOI: **10.3390/ijms10114772**.

27 D. Coates, The effect of lateral substitution on smectic C formation, *Liq. Cryst.*, 1987, **2**(4), 423–428, DOI: **10.1080/02678298708086299**.

28 M. S. Silberberg, *The Molecular Nature of Matter and Change*, McGraw-Hill, 4th edn, 2006.

29 P. Berdague, J. P. Bayle, M. S. Ho and B. M. Fung, New laterally aromatic branched liquid crystal materials with large nematic ranges, *Liq. Cryst.*, 1993, **14**(3), 667–674, DOI: **10.1080/02678299308027746**.

30 H. A. Ahmed, M. M. Naoum and G. R. Saad, Mesophase behavior of 1:1 mixtures of 4-*n*-alkoxyphenylazo benzoic acids bearing terminal alkoxy groups of different chain lengths, *Liq. Cryst.*, 2016, **43**(9), 1259–1267, DOI: **10.1080/02678292.2016.1166528**.

31 G. Y. Yeap, H. C. Lee, W. A. K. Mahmood, C. T. Imrie, D. Takeuchi and K. Osakada, Synthesis, thermal and optical behavior of non-symmetric liquid crystal dimers α-(4-benzylidene-substituted-aniline-4′-oxy)-ω-[pentyl-4-(4′-phenyl)benzoateoxy]hexane, *Phase Transitions*, 2011, **84**(1), 29–37, DOI: **10.1080/01411594.2010.513613**.

32 N. Mardirossian and M. H. Gordan, Thirty years of density functional theory in computational chemistry: an overview and extensive assessment of 200 density functionals, *Mol. Phys.*, 2017, **115**, 2315–2372, DOI: **10.1080/00268976.2017.1333644**.

33 M. J. Frisch, G. W. Trucks, H. B. Schlegel, G. E. Scuseria, M. A. Robb, J. R. Cheeseman, G. Scalmani, V. Barone, B. Mennucci, G. A. Petersson, H. Nakatsuji, M. Caricato, X. Li, H. P. Hratchian, A. F. Izmaylov, J. Bloino, G. Zheng, J. L. Sonnenberg, M. Hada, M. Ehara, K. Toyota, R. Fukuda, J. Hasegawa, M. Ishida, T. Nakajima, Y. Honda, O. Kitao, H. Nakai, T. Vreven, J. A. Montgomery, J. E. Peralta, F. Ogliaro, M. Bearpark, J. J. Heyd, E. Brothers, K. N. Kudin, V. N. Staroverov, R. Kobayashi, J. Normand, K. Raghavachari, A. Rendell, J. C. Burant, S. S. Iyengar, J. Tomasi, M. Cossi, N. Rega, J. M. Millam, M. Klene, J. E. Knox, J. B. Cross, V. Bakken, C. Adamo, J. Jaramillo, R. Gomperts, R. E. Stratmann, O. Yazyev, A. J. Austin, R. Cammi, C. Pomelli, J. W. Ochterski, R. L. Martin, K. Morokuma, V. G. Zakrzewski, G. A. Voth, P. Salvador, J. J. Dannenberg, S. Dapprich, A. D. Daniels, O. Farkas, J. B. Foresman, J. V. Ortiz, J. Cioslowski and D. J. Fox, *Gaussian 09, Revision D.01*, Wallingford CT, 2009.